NeuroImage 233 (2021) 117969

Contents lists available at ScienceDirect

NeuroImage

journal homepage: www.elsevier.com/locate/neuroimage

Measuring the cortical tracking of speech with optically-pumped magnetometers

Paul de Lange[a], Elena Boto[b], Niall Holmes[b], Ryan M. Hill[b], Richard Bowtell[b], Vincent Wens[a,c], Xavier De Tiège[a,c], Matthew J. Brookes[b], Mathieu Bourguignon[a,d,e,*]

[a] Laboratoire de Cartographie fonctionnelle du Cerveau, UNI – ULB Neuroscience Institute, Université libre de Bruxelles (ULB), 808 Lennik Street, Brussels 1070, Belgium
[b] Sir Peter Mansfield Imaging Centre, School of Physics and Astronomy, University of Nottingham, University Park, Nottingham NG7 2RD, United Kingdom
[c] Department of Functional Neuroimaging, Service of Nuclear Medicine, CUB Hôpital Erasme, Université libre de Bruxelles (ULB), Brussels, Belgium
[d] Laboratory of neurophysiology and movement biomechanics, UNI – ULB Neuroscience Institute, Université libre de Bruxelles (ULB), Brussels, Belgium
[e] BCBL, Basque Center on Cognition, Brain and Language, San Sebastian 20009, Spain

ARTICLE INFO

Keywords:
Cortical tracking of speech
MEG
Optically pumped magnetometer

ABSTRACT

During continuous speech listening, brain activity tracks speech rhythmicity at frequencies matching with the repetition rate of phrases (0.2–1.5 Hz), words (2–4 Hz) and syllables (4–8 Hz). Here, we evaluated the applicability of wearable MEG based on optically-pumped magnetometers (OPMs) to measure such cortical tracking of speech (CTS). Measuring CTS with OPMs is *a priori* challenging given the complications associated with OPM measurements at frequencies below 4 Hz, due to increased intrinsic interference and head movement artifacts. Still, this represents an important development as OPM-MEG provides lifespan compliance and substantially improved spatial resolution compared with classical MEG.

In this study, four healthy right-handed adults listened to continuous speech for 9 min. The radial component of the magnetic field was recorded simultaneously with 45–46 OPMs evenly covering the scalp surface and fixed to an additively manufactured helmet which fitted all 4 participants. We estimated CTS with reconstruction accuracy and coherence, and determined the number of dominant principal components (PCs) to remove from the data (as a preprocessing step) for optimal estimation. We also identified the dominant source of CTS using a minimum norm estimate.

CTS estimated with reconstruction accuracy and coherence was significant in all 4 participants at phrasal and word rates, and in 3 participants (reconstruction accuracy) or 2 (coherence) at syllabic rate. Overall, close-to-optimal CTS estimation was obtained when the 3 (reconstruction accuracy) or 10 (coherence) first PCs were removed from the data. Importantly, values of reconstruction accuracy (~0.4 for 0.2–1.5-Hz CTS and ~0.1 for 2–8-Hz CTS) were remarkably close to those previously reported in classical MEG studies. Finally, source reconstruction localized the main sources of CTS to bilateral auditory cortices. In conclusion, t

his study demonstrates that OPMs can be used for the purpose of CTS assessment. This finding opens new research avenues to unravel the neural network involved in CTS across the lifespan and potential alterations in, e.g., language developmental disorders. Data also suggest that OPMs are generally suitable for recording neural activity at frequencies below 4 Hz provided PCA is used as a preprocessing step; 0.2–1.5-Hz being the lowest frequency range successfully investigated here.

1. Introduction

It is increasingly recognized that brain oscillations play a crucial role in speech processing (Meyer, 2018). Specifically, during continuous speech listening, auditory cortical oscillations track the temporal fluctuations of the speech temporal envelope at frequencies matching with the repetition rates of phrases, words and syllables (Ahissar et al., 2001; Bourguignon et al., 2013; Broderick et al., 2017; Destoky et al., 2019b; Di Liberto et al., 2015; Ding et al., 2017; Ding and Simon, 2014; Gross et al., 2013; Horton et al., 2013; Keitel et al., 2018; Kösem and van Wassenhove, 2016; Luo and Poeppel, 2007; Meyer and Gumbert, 2018; Molinaro et al., 2016; Müller et al., 2018; O'Sullivan et al., 2014; Peelle et al., 2013; Pellegrino et al., 2011; Puschmann et al., 2017). Such cortical tracking of speech (CTS) is thought to reflect speech pars-

* Corresponding author.
E-mail addresses: mathieu.bourguignon@ulb.ac.be, mabourgu@ulb.ac.be (M. Bourguignon).

https://doi.org/10.1016/j.neuroimage.2021.117969
Received 17 August 2020; Received in revised form 8 January 2021; Accepted 4 March 2021
Available online 17 March 2021

ing or chunking, which are essential steps supporting subsequent speech recognition (Meyer, 2018).

Only two non-invasive electrophysiological brain recording methods provide the temporal resolution needed to estimate CTS: magnetoencephalography (MEG) and electroencephalography (EEG). For the purpose of CTS estimation in adults, MEG is clearly superior to EEG as it requires about 3 times less recording time than EEG to yield significant results (Destoky et al., 2019b). But classical MEG systems built with superconducting quantum interference devices (SQUIDs) come with two major drawbacks. (*i*) They offer a single fixed-size helmet, making them poorly suited to lifespan studies since sensors are sited further away from children's brains than adults' brains (R.M. Hill et al., 2019). (*ii*) Because sensors are immersed in liquid helium, they must be sited at least 2 cm away from the external surface of the helmet, which limits the sensitivity and spatial resolution of the technique (Boto et al., 2016; Iivanainen et al., 2017). Additionally, this head-to-helmet gap can be inhomogeneous, typically resulting in increased brain-to-sensor distance over the frontal region (Coquelet et al., 2020). In several applications, such as investigation of developmental language disorders, it would be desirable to measure CTS optimally (i.e., with MEG) without introducing head-size biases, and with optimal spatial resolution.

The miniaturization and commercialization of optically pumped magnetometers (OPMs) (Budker and Jackson Kimball, 2013; Budker and Romalis, 2007; Shah and Wakai, 2013), has enabled the development of OPM-MEG (Borna et al., 2017; Boto et al., 2018; Colombo et al., 2016). OPM-MEG addresses some of the drawbacks of SQUID-MEG. In contrast with SQUIDs, OPMs do not require cryogenic cooling, which has opened the possibility of mounting light-weight, wearable sensors on a flexible, sizable cap, much like in EEG (Boto et al., 2017 2018, 2019; Hill et al., 2020). And because this setup allows for on-scalp MEG recording, the spatial resolution and sensitivity to neural sources is improved significantly (Boto et al., 2016; Iivanainen et al., 2017). These advantages make OPM the perfect candidate for performing CTS analyses in studies involving children.

While it is a very promising technique that has already reproduced results obtained with SQUID-MEG, the development of OPM-MEG is still ongoing. It is not yet fully understood under what circumstances the technique is adequate or optimally reliable (Tierney et al., 2019a, 2019b). Small groups of OPMs placed over targeted brain regions have been applied in studies of sensorimotor processes in the 5–100-Hz frequency range (Borna et al., 2017; Lin et al., 2019; Wyllie et al., 2012; Xia et al., 2006), cognitive functions in the 4–8-Hz (Barry et al., 2019) and 15–30-Hz frequency ranges (Tierney et al., 2018), and used to measure gamma-band activity (> 30 Hz) in visual cortices (Iivanainen et al., 2020b). Recently, a whole-head OPM-MEG system with 49 sensors (as used in this study) has also been developed and applied in the simultaneous study of beta-band sensorimotor and gamma-band visual activity (Hill et al., 2020). However, to date there has been no report on the functionality of OPMs for frequencies below 4 Hz. For OPMs to be suitable for CTS investigations, they should perform in frequency ranges matching with the repetition rate of phrases (0.2–1.5 Hz), words (2–4 Hz) and syllables (4–8 Hz). There are multiple artifacts that could disturb measurements in that frequency range: head-movement and sensor-movement being the most notable (Holmes et al., 2018). It is conjectured however, that with the currently employed technique of active shielding, minor instances of such artifacts should be tolerable (Holmes et al., 2018; Iivanainen et al., 2019), at least if adequate preprocessing techniques are used.

In light of the above, this proof of concept study evaluates the applicability of OPM-MEG to measure CTS at the individual level in a small sample of healthy adults. To optimize comparability with existing literature, CTS is quantified with the two methods commonly used in the field: (*i*) a cross-validated ridge-regression approach to estimate the reconstruction accuracy of speech envelope from MEG signals (Crosse et al., 2016; Ding and Simon, 2012; Mesgarani et al., 2009), and (*ii*) coherence analysis (Halliday et al., 1995) to estimate the linear dependence between MEG and speech temporal envelope signals in the frequency domain (Bourguignon et al., 2013; Destoky et al., 2019b; Vander Ghinst et al., 2016). We assessed the ability of principal component analysis (PCA) and independent component analysis (ICA) as preprocessing steps to overcome the large-amplitude, low-frequency artifacts expected to arise from head movements. We optimize the number of dominant principal components (PCs) removed from the data in the cross-validation framework of the reconstruction accuracy approach. Based on these optimal numbers of PCs to remove, we estimate the cortical generators of CTS in the coherence framework, as done in most studies in the field. Finally, we further evaluate the adequacy of the optimal number of PCs for coherence estimation. We hypothesised that with such preprocessing, CTS will be uncovered even at its lowest frequencies (phrasal, 0.2–1.5 Hz).

2. Methods

2.1. Participants

Four healthy adult human participants (1 female) took part in the experiment. They were aged 24 ± 1 years (mean ± SD). Three were native English speakers and one (participant 4) was a native German speaker. None of them had prior developmental, auditory, neurological, or psychiatric disorders, except for participant 4 who reported having a mild tinnitus. All were right-handed according to Edinburgh handedness inventory (Oldfield, 1971) (mean ± SD score, 83.3 ± 20.1).

This study was approved by the University of Nottingham Medical School Research Ethics Committee and participants signed a written informed consent before participation. They did not receive any financial compensation. The experiments took place at the University of Nottingham.

2.2. Experimental condition

Participants listened to a 9-min speech sound excerpt from an audiobook (male reader, Crime and Punishment; https://etc.usf.edu/lit2go/182/crime-and-punishment/). Sound was delivered at a comfortable hearing level through two speakers placed outside circular openings in two upper corners of the magnetically-shielded room (MSR), in which the OPM-MEG system is housed.

2.3. Data acquisition

Fig. 1 presents our OPM-MEG setup.

During the experimental condition, participants' brain activity was recorded with the whole-head, OPM-MEG system at the Sir Peter Mansfield Imaging centre (University of Nottingham, United Kingdom). For a full description of the recording procedure, see Hill et al. (2020). In brief, neuromagnetic signals were recorded using 46 (45 in participant 2) QuSpin OPMs (QuSpin Inc., Colorado, USA) evenly covering the scalp surface (Osborne et al., 2018). Sensors were mounted on a rigid, additively manufactured helmet at known positions relative to the helmet surface. A mapping from the helmet surface to the head surface was achieved using optical scanning and a coregistration procedure described in Hill et al. (2020). This enabled complete knowledge of OPM sensor location and orientation relative to brain anatomy. Brain anatomy was acquired via anatomical magnetic resonance images (MRI), using a 3- T Philips Ingenia system, running an MPRAGE sequence, at an isotropic spatial resolution of 1 mm. OPMs were oriented so as to measure the component of the magnetic field approximately normal to the scalp. The recordings were performed in a MSR designed and built specifically for OPM-MEG recordings (MuRoom, Magnetic Shields Limited, Kent, UK). To further limit the interference induced by head movements, background field and gradients were reduced by a factor of ~3 using a set of bi-planar coils placed either side of the participant (Holmes et al., 2018, 2019). MEG signals were low-pass filtered at

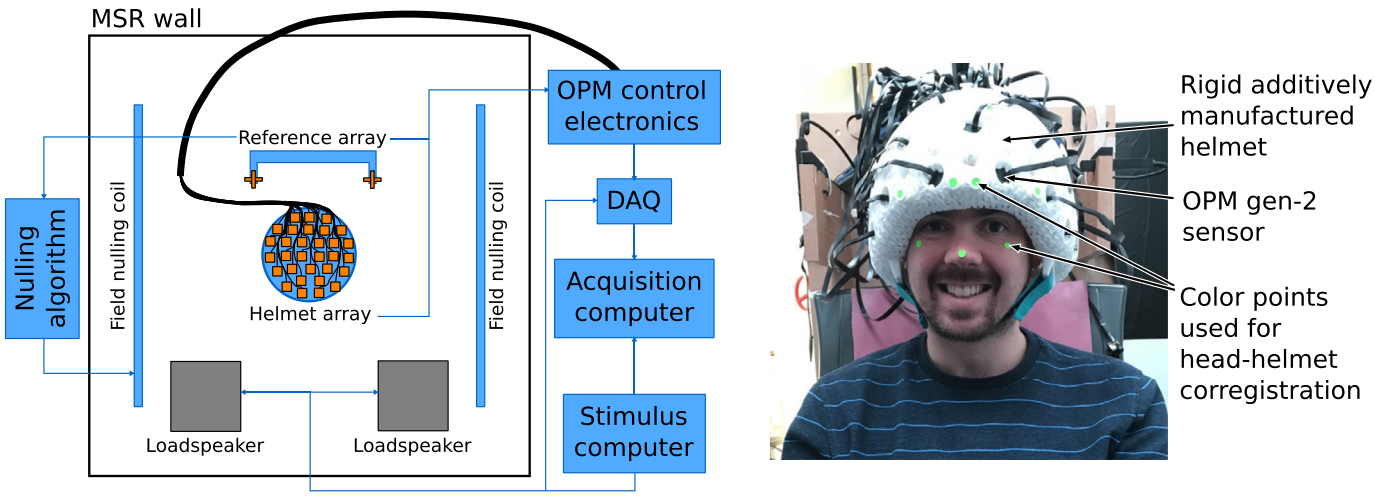

Fig. 1. OPM-MEG setup. *Left* — Schematic diagram of the whole system (adapted from Hill et al., 2020). Field nulling coils lowered the background field and gradients. Sound signals were fed to two speakers as well as to the DAQ used to record OPM-MEG signals for synchronization purposes. *Right* — Participant wearing the OPM-MEG helmet. Brain activity was recorded with 45–46 OPMs gen-2 sensors placed on a rigid additively manufactured helmet. Color points were placed on the participants and on the helmet for subsequent head–helmet coregistration with a 3-dimensional optical imaging system (Hill et al., 2020). (For interpretation of the references to colour in this figure legend, the reader is referred to the web version of this article.)

500 Hz and sampled at 1200 Hz by a National Instruments (Texas, USA) data acquisition system. The audio signal was simultaneously sampled with the MEG data and used to synchronize the original sound track (sampled at 44,100 Hz) with MEG signals.

2.4. Data preprocessing

The analysis of the data was carried out with the use of custom MATLAB scripts.

Continuous MEG data were band-pass filtered at 0.2–45 Hz. For a wearable system where the helmet is allowed to move with the head, very low frequency neuromagnetic signals are typically contaminated by movement artifacts (similar across sensors). We relied on principal component analysis (PCA) to remove a few dominant principal components (PCs) in order to attenuate this interference. As it was unclear how many PCs should be removed, we deferred this choice to a later stage (see subSection 2.5), where an optimal number is automatically selected in a cross-validation loop. Hence, several versions of the preprocessed data were estimated, where the first $n = 0, 1, 2, \ldots$ 10 PCs were removed.

In a separate analysis, we preprocessed the OPM-MEG signals with independent component analysis (ICA). Twenty independent components were evaluated from the MEG data low-pass filtered at 25 Hz using FastICA algorithm (dimension reduction, 25; non-linearity, tanh) (Hyvärinen et al., 2001; Vigario et al., 2000). Independent components corresponding to eyeblink, eye movement, heart bead and head movement artifacts were subtracted from the full band and full rank MEG data.

Finally, we also considered the data minimally preprocessed (no ICA or PCA), and the data preprocessed with both ICA and PCA.

Time points at timings 1-s around remaining artifacts were set to bad and corresponding data were not used in further analyses. To identify artifacts, MEG amplitude was estimated as the rectified signal low-pass filtered at 1 Hz, and further standardized (i.e., converted to a z-score). Data were considered contaminated by artifacts when z-scored amplitude for at least one MEG channel was above 5. This led to disregarding 14 ± 5% of the data (mean ± SD across participants and number of removed PCs; range 5–22%)

We finally extracted the temporal envelope from the audio signal. To that aim, the audio signal was rectified and low-pass filtered at 50 Hz. We did not explore superior methods for extracting the speech envelope (Biesmans et al., 2017), but this is unlikely to affect the results as the resulting envelopes are very similar (Destoky et al., 2019b).

2.5. Sensor-level CTS assessed with reconstruction accuracy

A global value of phrasal (0.2–1.5 Hz), word (2–4 Hz) and syllabic (4–8 Hz) CTS was evaluated for all MEG signals at once using a ridge-regression approach with nested cross-validation. Note that since it is common in the literature to estimate CTS at 2–8 Hz (Broderick et al., 2017, 2019; Destoky et al., 2019a; Di Liberto et al., 2015, 2018; Ding and Simon, 2012; Lalor and Foxe, 2010; Mesgarani et al., 2009; O'Sullivan et al., 2014), we also estimated CTS in this combined word/syllabic frequency range. Using the mTRF toolbox (Crosse et al., 2016), we trained a decoder on MEG signals to reconstruct the speech temporal envelope, and estimated the Pearson correlation between this reconstruction and the real speech temporal envelope. This correlation is often referred to as the reconstruction accuracy, and it provides a global measure of CTS. A similar approach has been used in previous studies on CTS (Destoky et al., 2019b; Ding and Simon, 2012; Lalor and Foxe, 2010; O'Sullivan et al., 2014; Zion-Golumbic et al., 2013).

In practice, MEG signals were band-pass filtered at phrasal, word, syllabic and word/syllabic frequencies, resampled to 10 Hz (phrasal CTS) or 40 Hz (word and syllabic CTS) and standardized. A decoder was built based on MEG data from –500 ms to 1000 ms (phrasal CTS) or from 0 ms to 250 ms (word and syllabic CTS) with respect to speech temporal envelope. Filtering and delay ranges were as in previous studies (Destoky et al., 2019b; Ding and Simon, 2012; Lalor and Foxe, 2010; O'Sullivan et al., 2014; Zion-Golumbic et al., 2013). Regularization was applied to limit the norm of the derivative of the reconstructed speech temporal envelope (Crosse et al., 2016), by estimating the decoder for a fixed set of ridge values ($\lambda = 2^{-10}, 2^{-8}, 2^{-6}, 2^{-4}, 2^{-2}, 2^{\circ}$). The decoder was also estimated after having removed the first $n = 0, 1, 2, \ldots, 10$ PCs from MEG data (before applying band-pass filtering). In a classical 10-fold cross-validation approach, the data are split into 10 segments of equal length, the decoder is estimated for 9 segments and tested on the remaining segment, and this procedure is repeated 10 times until all segments have served as test segments. The ridge value and number of removed PCs yielding the maximum mean reconstruction accuracy are then retained. Due to the maximization procedure, ensuing reconstruction accuracy is inflated. To eliminate this bias, we adopted a 10-fold nested cross-validation scheme (Varoquaux et al., 2017). Following that

scheme, for each segment, a 9-fold cross validation was conducted on the remaining 9 segments to select the ridge value and number of removed PCs that maximize the reconstruction accuracy, and the corresponding decoder was used to estimate the reconstruction accuracy for that segment. This procedure led to 10 values of reconstruction accuracy and 10 numbers of first PCs removed from the data (one for each segment) for each participant and frequency range investigated. We then estimated the mean and standard deviation of reconstruction accuracy, and the rounded mean of the number of removed PCs to which we refer as the optimal number of removed PCs.

In separate analyses, we also assessed the reconstruction accuracy for the data not preprocessed with PCA, for the data preprocessed with ICA only, and for the data preprocessed with ICA and then PCA. Hence, in the analyses not involving PCA, there was no optimization on the number of PCs removed.

2.6. Temporal response functions

We estimated the temporal response functions of OPM–MEG signals associated to speech temporal envelope with the mTRF toolbox (Crosse et al., 2016). The approach was similar to that used to estimate reconstruction accuracy, but this time, it was the speech temporal envelope that was used to reconstruct OPM–MEG signals, giving rise to coefficients that can be interpreted as the deconvoluted brain response to continuous speech, i.e., a temporal response function akin to an evoked response in trigger-based experiments. Temporal response functions were obtained from the data preprocessed with PCA, with the optimal number of PCs removed (identified in the reconstruction accuracy analysis) and not preprocessed with ICA.

OPM–MEG signals were filtered as in the previous subsection, and downsampled resampled to 20 Hz (phrasal CTS) or 100 Hz (word and syllabic CTS) and standardized. For each subject and OPM–MEG signal, the temporal response function was modeled from –700 ms to 1200 ms (phrasal CTs) or –100 ms to 350 ms (word and syllabic CTs). The optimal ridge value was selected (from among the same ridge values as in previous subsection) with a tenfold cross-validation procedure to maximize the maximum across sensors of the correlation between original OPM–MEG signals and those reconstructed as the convolution of the temporal response function with speech temporal envelope. Temporal response functions were recomputed based on all the available data for the selected ridge value.

2.7. Sensor-level CTS assessed with coherence

We calculated the coherence-based CTS as the coherence between speech temporal envelope and each of the MEG signals, with and without ICA preprocessing, and after correction by removal of the first $n = 0$, 1, 2, …, 10 PCs from MEG data (note that *a posteriori*, we did this for n up to 20). To that aim, time-locked MEG and speech temporal envelope signals were segmented into 2000-ms epochs with 1600-ms overlap, affording a 0.5-Hz frequency resolution (Bortel and Sovka, 2014). Epochs contaminated by artifacts were discarded from the analysis. Coherence was evaluated only for frequencies below 10 Hz, which are critical for speech comprehension (Rosen, 1992), following the classical formulation of coherence analysis (Halliday et al., 1995). Note that the framework of coherence analysis also provided us with linear spectral densities. Furthermore, we specifically analysed coherence values in the three frequency ranges of interest introduced in subSection 2.5: phrasal frequencies (mean coherence across 0.2–1.5 Hz), word frequencies (2–4 Hz) and syllable frequencies (4–8 Hz). The 2–8-Hz frequency range was not explored with coherence analysis since this is not typically done in the literature.

In the results section, we mainly focus on coherence and linear spectral densities estimated after having removed from the data the number of first PCs deemed optimal for the estimation of reconstruction accuracy.

To characterize the PCs that were—and were not—removed, we use the same analysis as described above in this subsection to estimate the linear spectral densities of the 20 first PCs, and their coherence with speech temporal envelope.

2.8. Source-level CTS assessed with coherence

The MEG forward models (mapping source activity onto MEG signals) were next computed within a 5-mm grid source space for 3 orthogonal source orientations per grid point with fieldtrip (Oostenveld et al., 2011). Forward modeling was based on the “single shell” method (Nolte, 2003). Based on these forward models, we computed a Minimum-Norm-Estimate (MNE) inverse solution (Dale and Sereno, 1993), with the regularization parameter fixed assuming a signal-to-noise ratio (SNR) of 1 (Hämäläinen et al., 2010). We then used this inverse solution embedded in the dynamic imaging of coherent sources approach (DICS; Gross et al., 2001) to produce coherence maps in the source space for each participant and frequency range investigated (phrasal, word and syllabic), and using the optimal number of removed PCs. Notably, the coherence value at each source location was optimized across the two source orientations (Bourguignon et al., 2015).

2.9. Group analysis

A non-linear transformation from individual MRIs to the MNI brain (“Montreal Neurological Institute”) was first computed using the spatial normalization algorithm implemented in Statistical Parametric Mapping (SPM12; Ashburner et al., 1997; Ashburner and Friston, 1999) and then applied to the coherence maps. The resulting maps were then averaged across participants to produce group-averaged maps.

We identified the coordinates of the global maximum within each hemisphere in group-averaged coherence maps. We only report on global coherence maxima and disregard the extent of the clusters of significant coherence. Indeed, cluster extent is hardly interpretable in view of the inherent smoothness of MEG source reconstructions (Bourguignon et al., 2017; Hämäläinen and Ilmoniemi, 1994; Hari et al., 1988; Sekihara et al., 2005; Wens et al., 2015).

2.10. Statistical analyses

2.10.1. Significance and comparison of CTS assessed with reconstruction accuracy

For each participant and frequency range investigated, we determined the significance of CTS assessed with reconstruction accuracy with a one sample t-test across the 10 validation runs.

The same approach was used to compare CTS values estimated for the data with vs. without PCA preprocessing, and for the data with vs. without ICA preprocessing.

2.10.2. Significance of CTS assessed with coherence analysis

For each participant and frequency range investigated (and number of PCs removed from the data), we determined the significance of CTS assessed with coherence with maximum-based statistics derived from surrogate data, which takes into account both the multiple comparisons across channels and the temporal autocorrelation within signals. For each participant, 1000 surrogate coherence distributions across channels were generated, as was done for genuine coherence values but with the audio signal replaced by Fourier-transform surrogates, which preserves the power spectrum by replacing the phase of Fourier coefficients by random numbers in the range $[-\pi; \pi]$ (Faes et al., 2004). Then, the maximum coherence value across all channels was extracted for each surrogate simulation. Finally, the 95^{th} percentile of this maximum coherence value yielded the coherence threshold at $p < 0.05$.

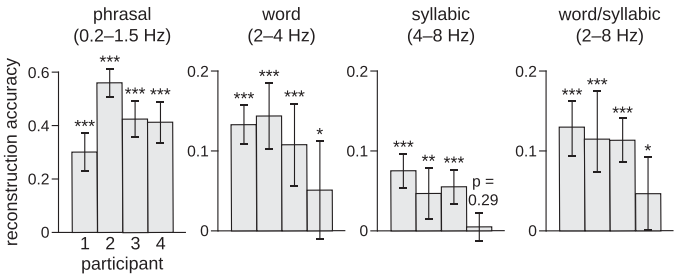

Fig. 2. CTS assessed with reconstruction accuracy. Displayed are the mean and standard deviation of reconstruction accuracy across the 10 validation runs, for each participant (1 to 4) and for phrasal, word, syllabic and word/syllabic CTS. Significance level is indicated above each bar (*, $p < 0.05$; **, $p < 0.01$; ***, $p < 0.001$). Note that since reconstruction accuracy was assessed in a cross-validation framework, it can take negative values and its expectation in the absence of coupling is 0.

Table 1
Mean ± standard deviation of reconstruction accuracy estimated from the data with or without ICA preprocessing and with or without PCA preprocessing.

	none	ICA	PCA	PCA and ICA
phrasal CTS	0.356±0.138	0.366±0.160	0.405±0.107	0.407±0.106
word CTS	0.106±0.041	0.112±0.043	0.104±0.053	0.104±0.033
syllabic CTS	0.047±0.038	0.041±0.044	0.039±0.028	0.043±0.025

2.10.3. Comparison between frequency ranges of MEG amplitude reduction for the optimal number of PCs removed from the data

We aimed to quantify the amount of noise reduction necessary to measure CTS optimally, and determine if such reduction depends on the frequency range investigated. To address that aim, we assessed the impact of optimal PCA preprocessing on MEG amplitude in the 3 frequency ranges investigated with a measure of amplitude reduction taken as the log-ratio of MEG amplitude before vs. after removal of the optimal number of PCs. The mean of this measure across all sensors was compared between frequency ranges with paired *t*-tests across the 4 participants.

2.11. Data and code availability

The data and analysis scripts underlying this report are available upon reasonable request from the corresponding author.

3. Results

CTS was quantified with two different measures (reconstruction accuracy and coherence), with the aim of determining the feasibility of OPM recordings to measure CTS, a type of coupling that involves frequencies lower than those previously explored with OPMs.

3.1. Reconstruction accuracy

Fig. 2 presents the values and significance of CTS at phrasal (0.2–1.5 Hz), word (2–4 Hz), and syllabic rates (4–8 Hz) quantified with reconstruction accuracy for the data preprocessed with PCA. CTS was significant in all 4 participants at phrasal and word rates, and in participants 1–3 at syllabic rate. In these estimations, the average number of PCs removed from the data was 7.3 ± 2.2 (participant 1 to 4: 8, 6, 5, 10) for phrasal CTS, 5.0 ± 2.9 (9, 2, 4, 5) for word CTS, and 3.5 ± 2.9 (3, 0, 4, 7) for syllabic CTS. Note that since it is common in the literature to estimate CTS at 2–8 Hz, we also present values for this frequency range in Fig. 2. For that frequency range, the average number of PCs removed from the data was 4.0 ± 1.4 (participant 1 to 4: 3, 3, 4, 6).

Table 1 presents the mean and standard deviation of reconstruction accuracy across participants for the data with or without ICA preprocessing and with or without PCA preprocessing. In ICA preprocessing, 2–4 components were regressed out of the data (participant 1 to 4: 2, 4, 4, 4). These components picked up eye blink or eye movements (1–2 components), heartbeat (0–1 component) or head movement (1–2 components) artifacts. When PCA was combined with (performed after) ICA, the number of PCs removed from the data was 5.0 ± 2.8 (participant 1 to 4: 5, 7, 1, 7) for phrasal CTS, 3.8 ± 2.1 (4, 1, 6, 4) for word CTS, and 4.3 ± 4.0 (1, 3, 3, 10) for syllabic CTS.

Table 1 clearly shows that ICA and PCA preprocessing were not crucial for estimation of reconstruction accuracy. First, including ICA preprocessing did not improve CTS estimation: at the participant level, CTS was not significantly higher when estimated from the data with vs. without ICA preprocessing (ICA vs. minimal preprocessing: all $p > 0.05$; combined ICA and PCA vs. PCA only: all $p > 0.05$ except for word CTS in participant 1 in favor of PCA only, $p = 0.0005$, $t_9 = 5.30$). Second, including PCA preprocessing improved CTS estimation at 0.2–1.5 Hz, but had virtually no effect at 2–4 Hz and 4–8 Hz: at the participant level, CTS was significantly higher when estimated from the data with vs. without PCA preprocessing in one participants at 0.2–1.5 Hz (PCA vs. minimal preprocessing: $p = 0.0003$, $t_9 = 5.30$; combined ICA and PCA vs. ICA only: $p = 0.0004$, $t_9 = 5.53$), but in none of the participants at 2–4 Hz and 4–8 Hz (all $p > 0.05$).

In sum, the impact of the different preprocessing methods on reconstruction accuracy was relatively limited, with a maximal reduction of less than 20% from minimal preprocessing to PCA only for syllabic CTS. Based on the above, and for the sake of simplicity, further analyses will mainly focus on CTS estimated from the data preprocessed with PCA only.

3.2. Temporal response functions

Fig. 3 presents the temporal response functions and corresponding topographies for phrasal, word and syllabic CTS. The temporal response functions were estimated from the data preprocessed with PCA with the number of PCs removed deemed optimal for the estimation of reconstruction accuracy.

In line with previous studies (Bourguignon et al., 2020; Broderick et al., 2017; Park et al., 2015), the temporal response functions at 0.2–1.5 Hz peaked at ~0 ms and 400–500 ms, more convincingly so in participants 2–4. Also in line with the literature (Destoky et al., 2019b; Ding and Simon, 2012; Lalor and Foxe, 2010; O'Sullivan et al., 2014; Zion-Golumbic et al., 2013), the temporal response functions at 2–4 Hz peaked at ~100 ms; those at 4–8 Hz showed oscillations but no convincing peak, except in participant 3 at 40 ms, and perhaps in participant 1 at 50 ms.

In several instances, the topography associated to the temporal response functions disclosed clear dipolar field patterns (two lobes of opposite polarity next to each other), indicative of the presence of a cortical source right underneath (i.e., bilateral temporal areas) with an orientation on the line that separates the two lobes (Hämäläinen et al., 1993). As expected (Boto et al., 2016; Iivanainen et al., 2017), these field patterns were more focal than those typically seen in SQUID–MEG or EEG studies.

3.3. Coherence at the sensor level

Fig. 4 presents the spectra of CTS assessed with coherence and corresponding sensor topographies at phrasal, word and syllabic rates (for the data optimally preprocessed with PCA, as hinted by the reconstruction accuracy analysis).

A prominent spectral peak was clearly seen at 0.5, 1 or 1.5 Hz that even spread to the 2- and 2.5-Hz frequency bins. This spread is likely to contribute significantly to the value of CTS at 2–4 Hz. Besides, Fig. 4 clearly suggests the presence of significant coherence at 4–8 Hz in participants 1 and 3. These observations were confirmed statistically: coherence was significant in all participants and investigated frequency ranges (all $p < 0.02$), except in participant 2 and 4 for syllabic CTS (both

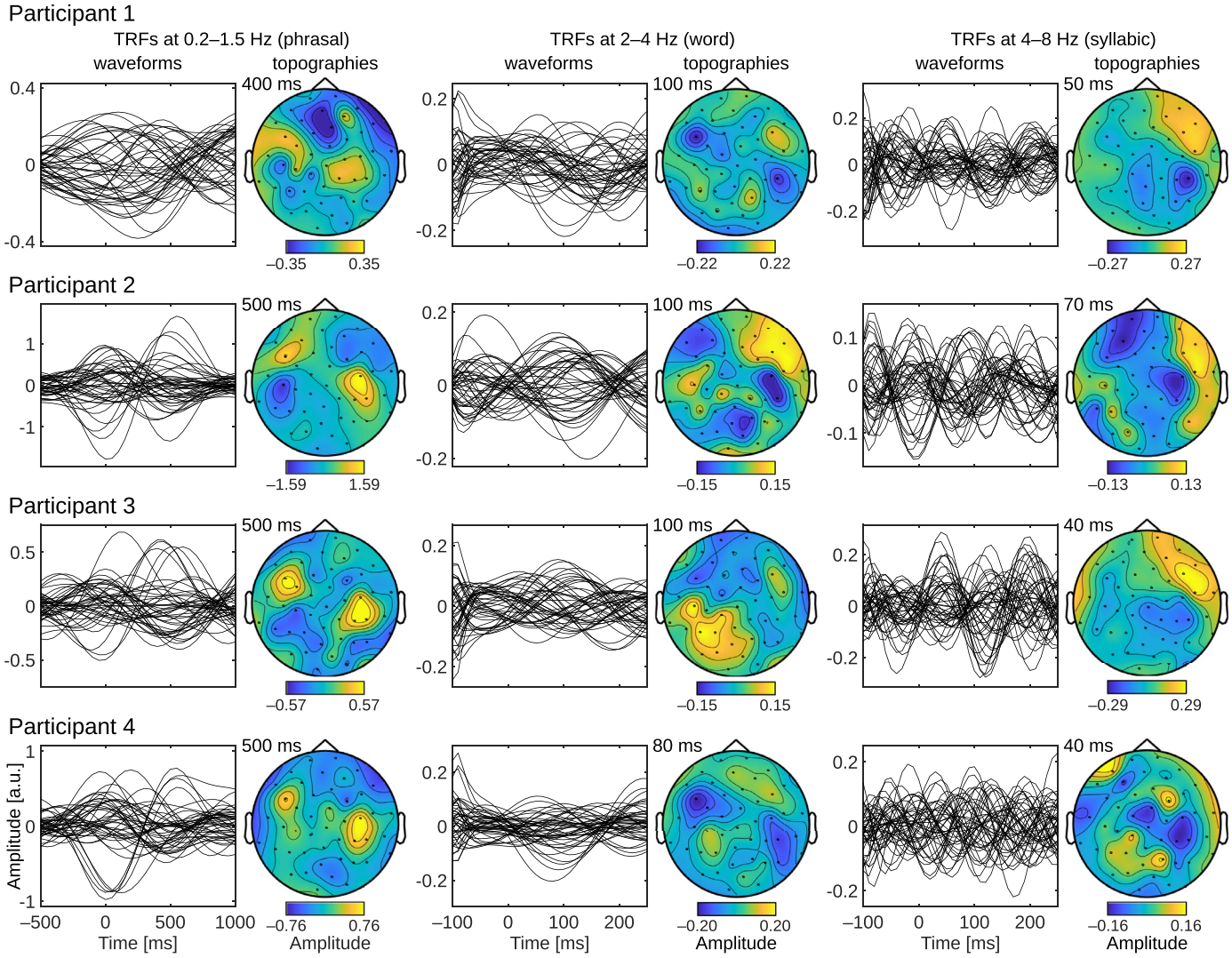

Fig. 3. Temporal response functions and associated topographies for phrasal, word and syllabic CTS. Temporal response functions (one trace per sensor) were computed for a number of removed PCs identified as optimal for the estimation of reconstruction accuracy. Sensor topographies were produced at timings indicated on the top left corner of each plot, which corresponded to a peak in the temporal response functions.

$p \approx 0.5$). Across subjects its values were 0.0759 ± 0.0584 (mean ± SD) at 0.2–1.5 Hz, 0.0145 ± 0.0044 at 2–4 Hz and 0.0065 ± 0.0019 at 4–8 Hz.

In sensor topographies, coherence was mostly dominant in sensors located above bilateral temporal areas, at locations corresponding with the lobes visible in topographies of the temporal response functions associated to speech envelope (see Fig. 3). Because coherence is always positive, the topographies for coherence are less straightforward to interpret than those for the temporal response functions.

3.4. Coherence at the source level

Fig. 5 presents the group-averaged source-level maps of CTS at phrasal, word and syllabic frequencies. In the 3 frequency ranges investigated, coherence displayed its global maximum in the right auditory cortex, and a second local maximum in the left auditory cortex. Coherence decreased monotonously with the distance to these local maxima in a large neighborhood, suggesting that we could resolve only one source of CTS per hemisphere.

Table 2 presents the coherence in both auditory cortices, showing some degree of right-hemisphere dominance for CTS. In individual coherence maps, phrasal and word CTS was right-hemisphere dominant in 3 out of 4 participants; syllabic CTS was right-hemisphere dominant in the 2 participants for whom it was statistically significant at the sensor level.

3.5. Impact of PCA preprocessing

Fig. 6 presents the linear spectral densities of MEG signals for a representative participant before and after removal of the optimal number of first PCs (here 6 PCs). Before PCs removal, MEG amplitude was at highest over the vertex. PCA preprocessing diminished this amplitude by a factor of ~10 at 0.2–1.5-Hz, ~5 at 2–4 Hz and ~3 at 4–8 Hz. Across participants, the mean across sensors of amplitude log-ratio (before vs. after removal of the optimal number of PCs) was 0.74 ± 0.17 (mean ± SD across participants) at 0.2–1.5 Hz, 0.38 ± 0.19 at 2–4 Hz and 0.19 ± 0.16 at 4–8 Hz. This shows that CTS estimation required more stringent power reduction below than above 2 Hz. And indeed, the mean across sensors of amplitude log-ratio was significantly higher at 0.2–1.5 Hz than at 2–4 Hz ($t_3 = 5.14$, $p = 0.014$) and 4–8 Hz ($t_3 = 9.83$, $p = 0.0022$). There was also a trend for the difference between 2–4 Hz and 4–8 Hz ($t_3 = 2.62$, $p = 0.079$).

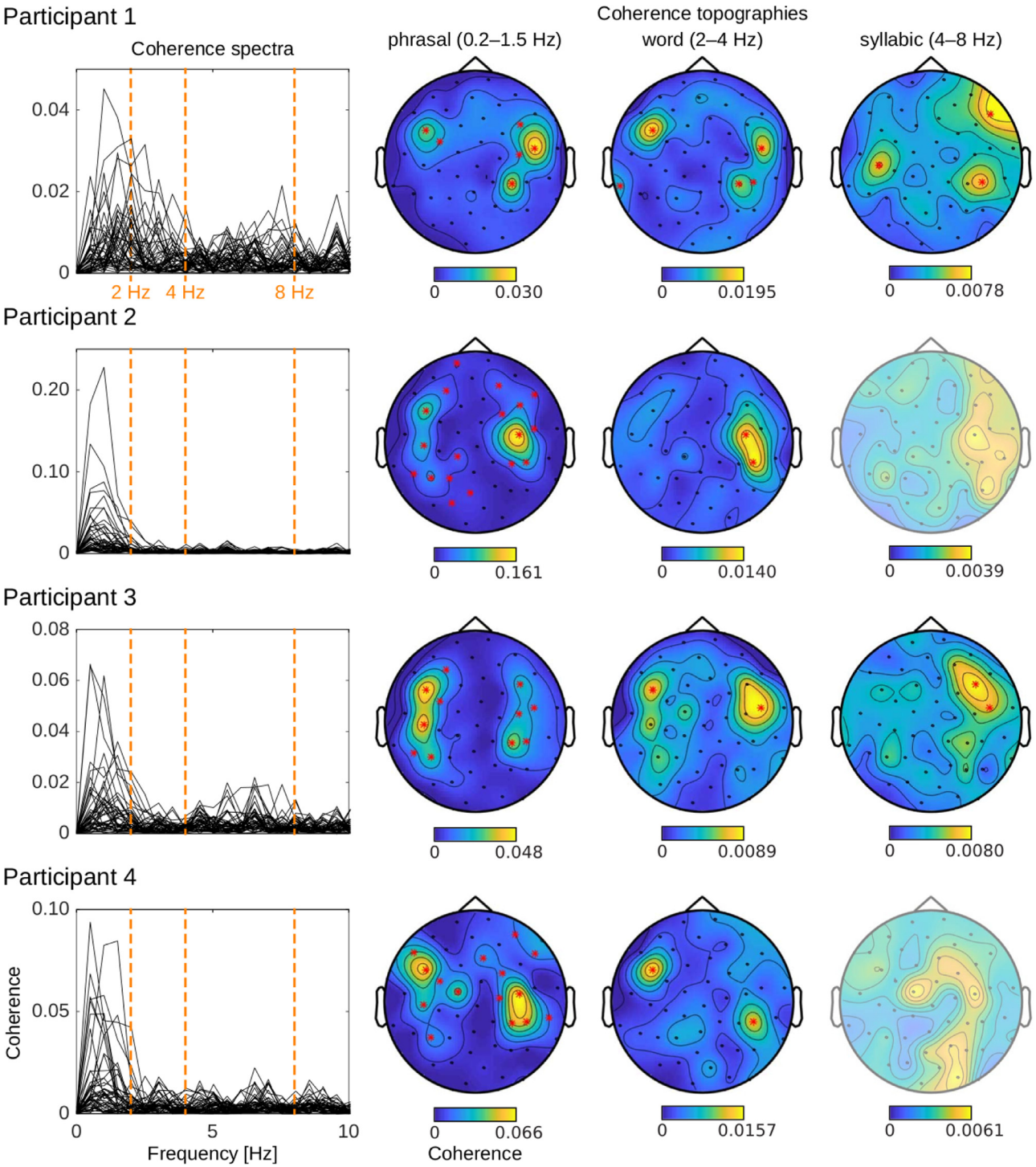

Fig. 4. Coherence spectra and topographies for each of the 4 participants. Coherence spectra (one trace per sensor) were computed for a different optimal number of removed PCs for the ranges 0–1.5 Hz, 2–4 Hz and 4.5–10 Hz. Coherence topographies were obtained by averaging the coherence across the frequency bins contained in 0.2–1.5 Hz, 2–4 Hz and 4–8 Hz. Sensors with significant coherence ($p < 0.05$) are indicated with a red asterisk. As coherence was not significant for syllabic CTS in participants 2 and 4, corresponding topographies are shaded. (For interpretation of the references to colour in this figure legend, the reader is referred to the web version of this article.)

Table 2
Coordinates and values of peak coherence in group-averaged source-level coherence maps.

	left hemisphere MNI coordinates [mm]	Coherence level	right hemisphere MNI coordinates [mm]	Coherence level
phrasal CTS	[−51 −14 17]	0.071	[53 −11 9]	0.101
word CTS	[−52 −13 10]	0.0142	[51 −2 17]	0.0217
syllabic CTS	[−47 −21 20]	0.0068	[38 −22 4]	0.0130

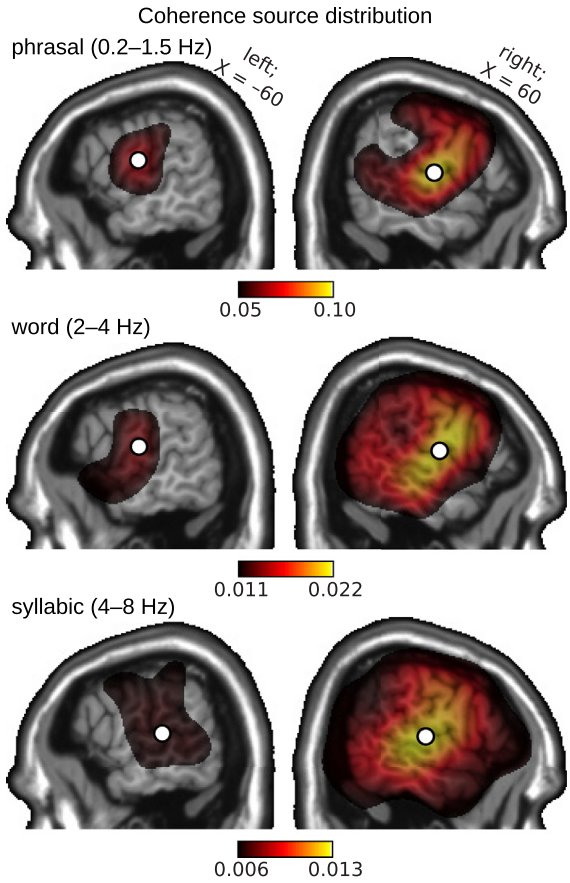

Fig. 5. Group-averaged source-level maps of CTS at phrasal (0.2–1.5 Hz), word (2–4 Hz) and syllabic (4–8 Hz) frequencies. CTS values were assessed with coherence, and thresholded at an arbitrary threshold of 50% of their maximum. CTS showed its two first local maxima (indicated with a white disk) at bilateral auditory cortices in the three frequency ranges investigated.

3.6. Optimal PCA preprocessing for coherence analysis

Fig. 7A illustres the crucial importance of PCA preprocessing for estimating CTS with coherence. It presents the maximum coherence across sensors for a number of removed PCs equal to 0, 1, 2,… 20. The curves indicate that a large amount of PCs should be removed to maximize the value of the coherence, with an optimum typically in between 10 and 15. For the sake of completeness, we also present these curves for reconstruction accuracy (see Fig. 7B). The limited impact of the number of removed PCs on these later curves confirms that PCA preprocessing was less important for CTS estimation with reconstruction accuracy. Nonetheless, the slight modulations induced by PCA on reconstruction accuracy was systematically beneficial at 0.2–1.5 Hz, either beneficial or neutral at 2–4 Hz and inconsistent at 4–8 Hz. CTS at 0.2–1.5 Hz and 2–4 Hz was largely stable for 3–15 PCs removed.

These results raise the question of how safe it is to remove as many as 10–15 PCs from the data. Is there a risk for removing relevant brain signals? To answer this question, we further characterized the first 20 PCs.

Fig. 8 presents the linear spectral densities of the PCs. All dominant components showed a monotonous amplitude decrease with frequency. Later components tended to display a spectral peak in the theta (4–8 Hz) or alpha (8–13 Hz) ranges. Qualitatively, the first component to show such spectral peaks was the 9th, 7th, 6th, and 11th for participants 1 to 4. Of the PCs that were removed in the cross-validation approach, only one showed such spectral peaks: in participant 1 for the estimation of word CTS.

Fig. 9 presents the values of coherence estimated between speech temporal envelope and the PCs. It shows that the cross-validation approach led to removing only a few PCs that were significantly coherent with the speech temporal envelope. In none of the cases (4 subjects times 3 frequency ranges) were the most coherent components removed. It also shows that the most coherent PCs were typically found after position 14 but that many significant components are seen before such cut off.

3.7. Reasonable preprocessing common to all frequency ranges

Last, we evaluated the adequacy of a fixed preprocessing scheme across frequency ranges and participants to investigate CTS with coherence analysis.

Figures S1–S6 present the spectra of CTS assessed with coherence and corresponding sensor topographies for data not preprocessed with ICA from which 0 (Fig. S1), 5 (Fig. S2) and 10 (Fig. S3) PCs were removed, and for the data preprocessed with ICA from which 0 (Fig. S4), 5 (Fig. S5) and 10 (Fig. S6) PCs were removed thereafter.

Clearly, it made little difference whether ICA was used as a preprocessing step, regardless of the number of PCs removed (compare Figs S1 vs. S4, S2 vs. S5, and S3 vs. S6).

With regard to PCA preprocessing, the results were overall better when removing 5 or 10 than 0 PCs, with just the exception of left-hemisphere CTS at 4–8 Hz in participant 1 that was significant only for 0 PCs removed. The differences between the results for 5 vs. 10 PCs removed were more subtle. Importantly, the peak CTS did not shift from one hemisphere to the other as more PCs were removed. The most notable difference was an increase in CTS at 0.5 Hz and 1 Hz when removing 10 compared to 5 PCs (see changes of the shape in the peak of CTS from Fig S2 to S3 and S5 to S6). Also worth mentioning is that left-hemisphere CTS at 2–4 Hz in participant 2 was reduced and became non-significant when moving from 5 to 10 PCs removed. The same happened for right-hemisphere CTS at 2–4 Hz in participant 4 but in this case, the changes were utterly subtle and only brought the p-value from one brink of the significance level to the other.

4. Discussion

This study demonstrates that OPM-MEG is able to identify significant CTS in relevant frequency ranges and with typical temporal dynamics. With appropriate preprocessing, prominent CTS at the lowest documented frequencies (0.2–1.5 Hz) was uncovered with OPM-MEG in the 4 participants tested. And even though the spatial coverage afforded by our 45–46 OPMs was somewhat limited (see Fig. 1), a classical source localization approach (MNE) was consistent with bilateral auditory cortices with some degree of right-hemisphere dominance as the dominant generators of CTS.

4.1. Comparability with previous CTS studies

Although we did not evaluate CTS with classical SQUID-MEG, comparison with previous studies indicates that the amplitude of CTS assessed with reconstruction accuracy derived from OPM-MEG recordings is similar to that derived from SQUID-MEG. Indeed, in a study using a very similar methodology (Destoky et al., 2019b), the mean reconstruction accuracy across 10 participants was ~0.4 at 0.2–1.5 Hz and ~0.1 at 2–8 Hz. These figures are strikingly similar to those we report here (see Table 1). Still, there are three main methodological differences between this SQUID-MEG study and ours, that should be mentioned. First, our results are based on 9 min of data while only 5 min of data were used in the SQUID-MEG study. The impact of this difference in recording duration was limited since reconstruction accuracy re-estimated based only on analysis of the 5 first minutes of our data was at most mildly diminished (0.36 at 0.2–1.5 Hz and 0.080 at 2–8 Hz; data not presented in

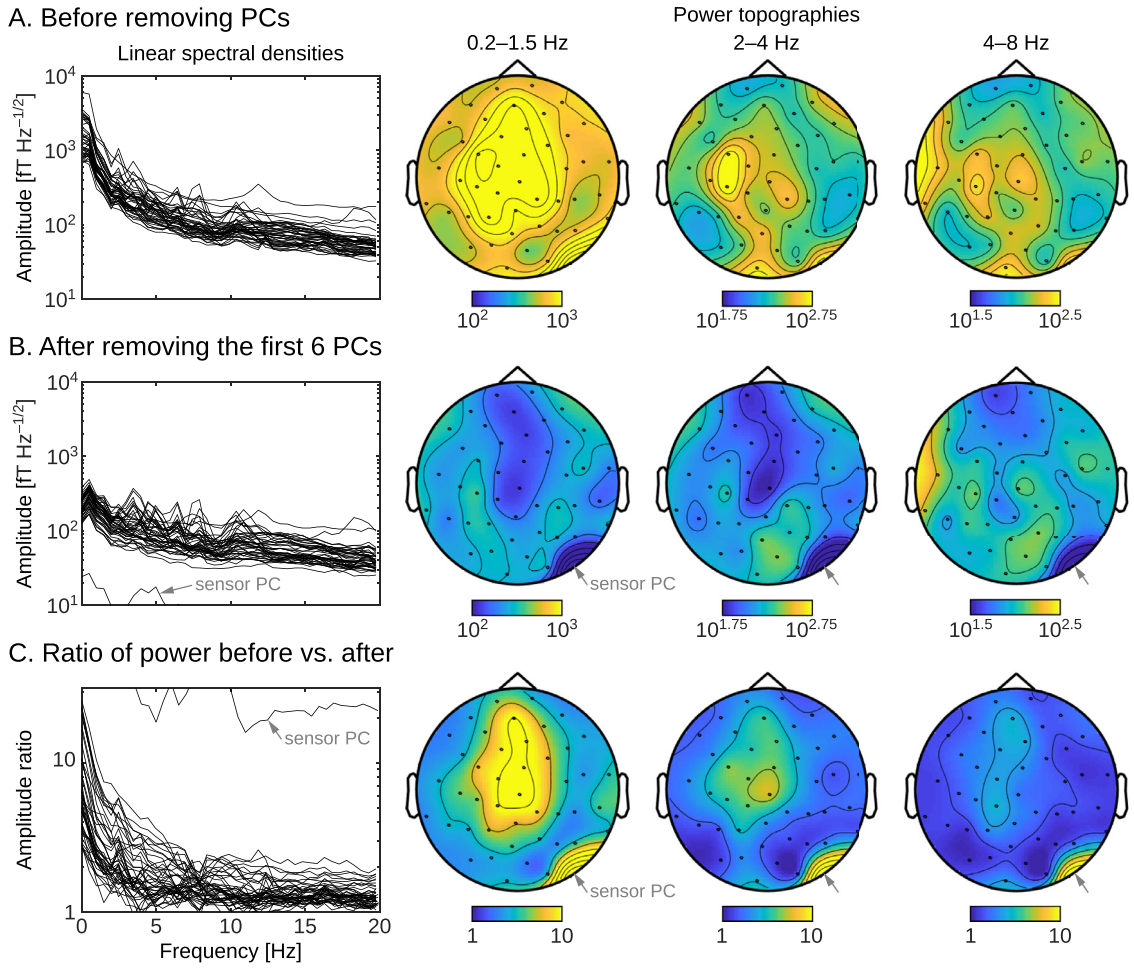

Fig. 6. OPM-MEG linear spectral densities from a representative participant (participant 2) and associated topographies at 0.2–1.5 Hz, 2–48 Hz and 4–8 Hz. A — Amplitude before removing principal components (PCs). B — Amplitude after removing the first 6 PCs, a number selected as optimal in the computation of reconstruction accuracy for 0.2–1.5-Hz CTS. C — Ratio of the amplitude, before vs. after, removal of the first 6 PCs. In this participant, one of the removed PCs closely matched with a single right occipital sensor. This is visible as an outlier trace in spectra B and C, and a blue or yellow patch in corresponding topographies, as indicated on the figure with gray arrows labelled "sensor PC". (For interpretation of the references to colour in this figure legend, the reader is referred to the web version of this article.)

the results section). Second, we incorporated an estimation of the optimal number of PCs to remove from the data in a nested cross-validation loop, whereas standard preprocessing (signal-space separation and independent component analysis) was used in the SQUID-MEG study. Third and last, this study was conducted in English while the SQUID-MEG study was conducted in French. The two later differences limit the comparability of our values of reconstruction accuracy with those in other studies. Nonetheless, the main finding holds that reasonable estimates of reconstruction accuracy can be obtained with OPM-MEG.

In contrast with the above, when estimated with coherence analysis, CTS magnitude was lower than that previously reported with SQUID-MEG. Indeed, still in the most comparable study (Destoky et al., 2019b), mean CTS magnitude across 10 participants was 0.19 at 0.5 Hz and 0.023 at 4–8 Hz, whereas it was ~3 times lower here (0.076 and 0.0065 respectively). Likely because of this decrease in coherence magnitude, 4–8-Hz CTS was not significant in 50% of the participants, which is low compared with the proportion of 80–90% reported in previous studies assessing CTS with coherence in the same way in more participants (10–20) and even with shorter (5-min) SQUID-MEG recordings (Destoky et al., 2019b; Vander Ghinst et al., 2016). The decrease in coherence-based CTS magnitude derived from OPM-MEG recordings could be due to reduced SNR in every channel or reduced spatial sampling, the latter having two consequences: it prohibits filtering based on spatial frequencies and it brings the risk of missing the best recording spot. To disentangle these possibilities future studies should estimate CTS based on both SQUID–MEG and OPM–MEG from the same participants and with a comparable number of sensors. No matter the origin of these reductions in coherence-based CTS magnitude, such reduction was not seen in reconstruction accuracy, likely because listed potential pitfalls were compensated for with model parameter optimization inherent to the reconstruction accuracy approach, but such optimization was not conducted in the coherence analysis. In support of this view, reconstruction accuracy was much less impacted by PCA preprocessing than coherence (see Fig. 7). Investigations with a larger number of sensors are likely to yield higher coherence values, thanks to increased coverage and possibility to adopt better preprocessing techniques such as signal space separation (Taulu et al., 2004, 2005) and its temporal extension (Taulu and Simola, 2006). The latter is especially interesting to deal with high-amplitude low-frequency artifacts such as those caused by magnetic objects worn by or implanted in participants (Bourguignon et al., 2016; Carrette et al., 2011; De Tiège et al., 2008; Kakisaka et al., 2013; Mäkelä et al., 2007; Song et al., 2009; Tanaka et al., 2009; Taulu and Hari, 2009). Since such artifacts are in essence movement artifacts, the temporal extension of signal space separation should deal equally

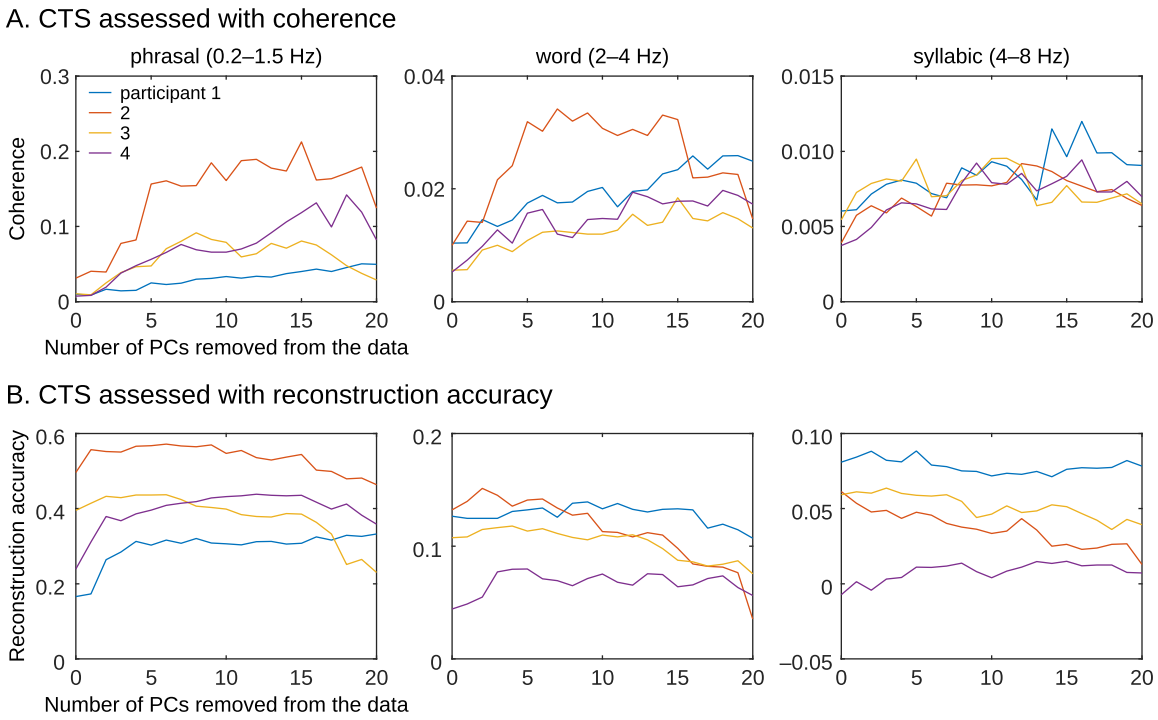

Fig. 7. Dependence of CTS estimated with coherence (A) and reconstruction accuracy (B) on the number of PCs removed from the data. For each participant (color-coded traces), the plots present the values for phrasal (left), word (middle) and syllabic (right) CTS. Traces in coherence plots indicate the maximum values of coherence across all sensors.

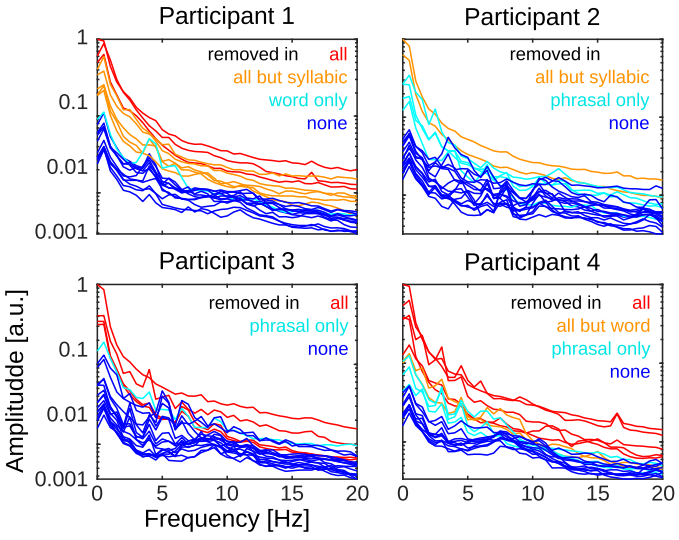

Fig. 8. Linear spectral densities of the first 20 PCs of OPM–MEG signals. Traces are color-coded for the number of times they were removed from the data prior to coherence estimation: red when removed for the estimation of phrasal, word and syllabic CTS, orange when removed in two instances, cyan when removed in one instance and blue when always retained. (For interpretation of the references to colour in this figure legend, the reader is referred to the web version of this article.)

efficiently with movement artifacts in OPM-MEG recordings. Another means to improve coherence estimation would be to record with OPMs mounted on a bespoke helmet rather than on rigid one-fit-all helmet as done here, simply because the bespoke setting makes it possible to record closer to the scalp and hence with a higher SNR (Boto et al., 2019; Hill et al., 2019, 2020). Similar improvement in SNR would be reached with a helmet in which sensors can be translated in the radial direction. The choice of the type of helmet is especially relevant here since in the setting we used, the distance between the sensors and the scalp was highest above the temporal lobes.

Source reconstruction localized the main sources of CTS to bilateral auditory cortices with some degree of right-hemisphere dominance. Although our sample was too small to assess statistically this effect, a right-hemisphere dominance is well in line with existing literature. Indeed, such right-hemisphere dominance is typically seen in ideal listening conditions, i.e., when speech sounds are not degraded and presented in a silent background (Bourguignon et al., 2013; Giraud and Poeppel, 2012; Gross et al., 2013; Luo and Poeppel, 2007; Peelle et al., 2013). But background noise compromises more right- than left-hemisphere CTS, so that in cocktail-party conditions (Cherry, 1953), CTS becomes left-hemisphere dominant (Destoky et al., 2019b; Power et al., 2012; Vander Ghinst et al., 2016, 2019). Studying CTS lateralization could provide some insights into a range of disorders such as, e.g., developmental dyslexia wherein atypical left/right hemispheric balance is suspected (Di Liberto et al., 2018; Hämäläinen et al., 2012; Lizarazu et al., 2015), and central auditory processing disorder, which is characterized by specific difficulties to comprehend speech in noise (Chermak et al., 1997). In light of this, being able to properly characterize the hemispheric dominance of CTS with OPM-MEG could be important for future applications.

4.2. OPM-MEG at frequencies below 4 Hz

So far, all OPM-MEG reports have focused on brain activity at frequencies above 4 Hz. Several technical challenges make it especially difficult to record OPM-MEG at frequencies below 4 Hz. Indeed, the noise floor (that is inherent to the sensor itself) of ~10 fT $Hz^{-1/2}$ at 10 Hz increases rapidly at lower frequencies, reaching ~20 fT $Hz^{-1/2}$ at 2 Hz and ~40 fT $Hz^{-1/2}$ at 0.5 Hz. These values remain however small compared with the ~1000 fT $Hz^{-1/2}$ we observed at 0.5 Hz in our experimental data (see Fig. 6). The dominant contribution to noise rather comes from movement artifacts that are made worse by the fact the sensors are free

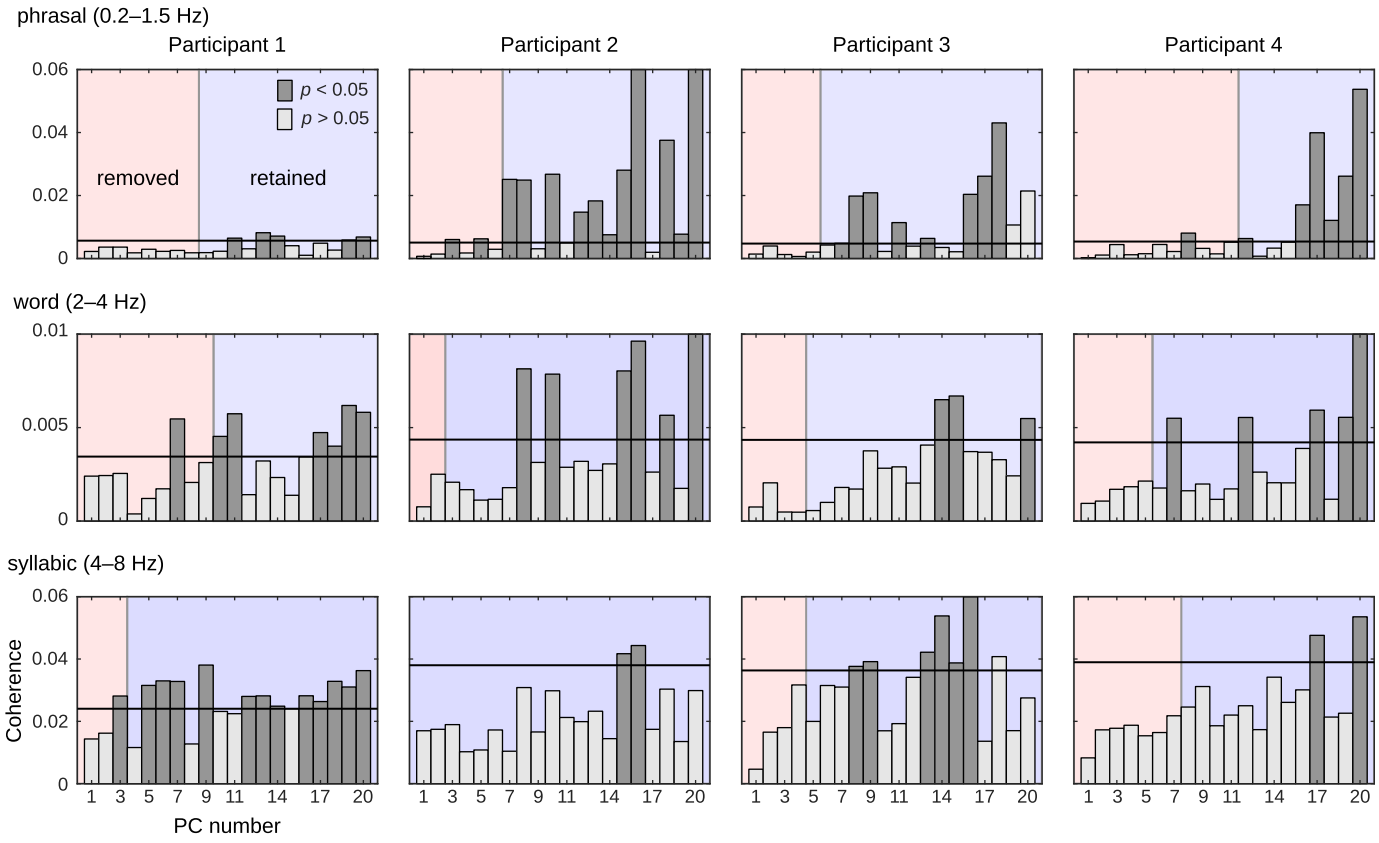

Fig. 9. Coherence between speech temporal envelope and the first 20 PCs of OPM–MEG signals. Coherence values are provided for each participant (arranged in columns) and each frequency range of interest (phrasal, word and syllabic; arranged in rows) as a function of the index of the PCs (the first being the one that explains the largest amount of variance in MEG signals). A horizontal line indicates the significance threshold at $p < 0.05$. Bars are dark gray for significant coherence values and light gray otherwise. A vertical line separates the PCs that were removed (light red background) from those that were retained (light blue background). (For interpretation of the references to colour in this figure legend, the reader is referred to the web version of this article.)

to move with the head. That is, because the ambient magnetic field is not exactly 0 inside the MSR, a sensor captures not just interference signals from external (and internal) sources, but also signals arising from rotation and translation in the spatially varying field as the head moves within the MSR. In our room, which is specifically designed and built for OPM-MEG investigations (Altarev et al., 2014), the remanent magnetic field amplitude following a degaussing procedure is ~1.5 nT and field gradients are less than 2 nT/m. These values are remarkably low compared with those in standard rooms used for SQUID-MEG, lower by a factor ~10 (Altarev et al., 2014; Hill et al., 2020). And a further reduction down to ~0.5 nT and ~1 nT/m is achieved with bi-planar compensation coils (Holmes et al., 2018, 2019). Even with these greatly reduced ambient fields, movements of 1 cm or rotations of 1° generate signals of up to ~10,000 fT and 9000 fT respectively. These figures are compatible with the large magnitude of low frequency MEG amplitude seen in unprocessed data (see Fig. 6).

Head movement artifacts share strong correlations across all sensors, lending themselves well to suppression with classical linear regression techniques such as PCA or ICA. This contrasts with more insidious muscle artifacts that are spatio-temporally complex (Muthukumaraswamy, 2013). Our results show that optimal CTS estimation is obtained after removing the first 3–5 (reconstruction accuracy) or 10–15 (coherence) PCs from the data, no matter whether ICA was included or not. The ICA was essentially dispensable since similar magnitudes and topographies of CTS were obtained regardless of its inclusion. This is probably due to that (*i*) large-amplitude head movement artifacts were easily removed by PCA anyway, and (*ii*) eye blink, eye movement and heartbeat artifacts had a relatively low amplitude and a limited spatial overlap with the genuine brain signals under scrutiny here. In contrast, PCA preprocessing was largely effective at boosting CTS estimated with coherence. Since removing PCs comes with a risk of removing genuine brain signals, it is desirable to project as little of the first PCs as possible, which would be about 3 (reconstruction accuracy) or 10 (coherence) based on our data. This said, removing 10 PCs would have led to discarding part—but certainly not most—of the signal of interest in most of our data. Indeed, in most of the participants and frequency ranges of interest, earlier components did show spectral modulations typical of brain signals (see Fig. 8) as well as significant coupling with speech temporal envelope (see Fig. 9). Still, PCA being a spatial projection method, it cannot alter the time course of brain responses. And keeping in mind coherence can be seen as a monotonous function of the signal to noise ratio, removing part of the signal is acceptable as far as at least as much noise is removed. In sum, our results indicate that it is reasonable to remove the 10 first PCs from the data in view of estimating CTS with coherence. Alternatively, it is possible to estimate the optimal number of PCs to remove in a data-driven way, following the cross-validation approach presented here for reconstruction accuracy. It is also straightforward to adapt this approach to coherence analysis, and to select a common preprocessing scheme for multiple frequency ranges by e.g., maximizing the—weighted—mean coherence across all considered frequency ranges. Finally, to minimize the quantity of genuine signals being projected out, one could also selectively remove the PCs that do not show significant coherence with speech temporal envelope.

4.3. Limitations and perspectives

The number of participants included in this study was limited. With only 4 participants, we did not deem it appropriate to assess the statistical significance of the group-level source-space map of CTS. Indeed, classical permutation tests in which genuine maps are randomly permuted with null maps do require a minimum of 5 participants in theory, and certainly more in practice to identify significant effects at $p < 0.05$ (Nichols and Holmes, 2002). We could have assessed the statistical significance of source-space maps with the same procedure used to assess sensor-level maps (Faes et al., 2004). However, sensor-level data already demonstrated the statistical significance of coherence bilaterally. In this sense, the demonstration of statistical significance—which was the objective of the present study—was already made. As we discuss in the next subsection, larger samples will have to be measured with denser OPM arrays to bring new insights into the neuronal network involved in CTS.

We did not track head position during the recording. In the setting we used, the OPM array was attached to the participant's head and hence moved with the participant's head. Accordingly, there was no need to track head position to determine where the sensors are with respect to brain sources as typically done in SQUID-MEG. However, information about head position could have helped improve the artifact rejection scheme by providing time series to regress out from the OPM time series (Stolk et al., 2013). In the same line, more advanced methods should be developed or adapted to improve artifact rejection, and increase the amount of data included in the analysis (i.e., about 15% of the data was discarded in our analyses). A particularly promising method to better disentangle movement artifacts from real signals could leverage recordings of the magnetic field in the 3 spatial directions (rather than just the radial component). Such method is currently under validation at the team of the University of Nottingham.

Further improvement of OPM technology and helmet design will make it possible to conduct OPM-MEG with increasingly more sensors simultaneously. These developments are needed to fully benefit from the increase in spatial resolution OPMs can afford. Indeed, to fully resolve spatially the scalp magnetic field generated by brain sources, it is necessary to keep the distance between neighboring sensors lower than the distance to the brain, which is roughly 1.5 cm (Ahonen et al., 1993). Such criterion would lead to measuring with about 300 sensors, which corresponds to the theoretical estimation of the number of degrees of freedom in MEG on-scalp distributions (Iivanainen et al., 2020a) notwithstanding the effect of sensor crosstalk which would need to be ameliorated to fully realize the potential of such a system (Nardelli et al., 2019). Naturally, even denser arrays would be needed to benefit from spatial filtering techniques (Taulu et al., 2004, 2005). Notwithstanding these considerations, our data demonstrates that 45–46 sensors was enough to localize the dominant source of CTS at locations consistent with bilateral auditory cortices.

CTS has recently proven very useful to further our understanding of the neural basis of dyslexia (Di Liberto et al., 2018; Molinaro et al., 2016; Thiede et al., 2020). These studies have consistently highlighted a deficit in CTS at phrasal frequencies, partly echoing the predictions of the temporal sampling framework for developmental dyslexia (Goswami, 2011; Goswami et al., 2014). The feasibility of OPM-MEG to study CTS opens new avenues to explore in greater details the alterations in CTS at the level of the neuronal network from childhood to adulthood as well as the developmental trajectory of speech-in-noise processing from childhood to adulthood (Vander Ghinst et al., 2019).

Conclusion

We have shown that OPM-MEG is a suitable tool to uncover CTS at all frequencies of interest, especially when the reconstruction accuracy approach is adopted. Thereby, we also provide the first demonstration of OPM suitability to measure brain activity at frequencies below 4 Hz.

Credit author statement

Paul de Lange: Methodology; Formal analysis; Data curation; Writing - Original Draft; Writing - Review & Editing

Elena Boto: Conceptualization; Methodology; Data curation; Writing - Review & Editing; Project administration

Niall Holmes: Conceptualization; Methodology; Writing - Review & Editing; Project administration

Ryan M. Hill: Methodology; Writing - Review & Editing

Richard Bowtell: Resources; Writing - Review & Editing

Vincent Wens: Methodology; Writing - Review & Editing

Xavier De Tiège: Conceptualization; Writing - Review & Editing; Supervision

Matthew J. Brookes: Conceptualization; Methodology; Resources; Writing - Review & Editing; Supervision; Funding acquisition

Mathieu Bourguignon: Conceptualization; Methodology; Formal analysis; Data curation; Writing - Original Draft; Writing - Review & Editing; Supervision; Funding acquisition

Data availability

The data and analysis scripts underlying this report are available upon reasonable request from the corresponding author.

Declaration of Competing Interest

E.B. and M.J.B. are directors of Cerca Magnetics Limited, a newly established spin-out company whose aim is to commercialize aspects of OPM-MEG technology, including the bi-planar coils used for field nulling. E.B., M.J.B., R.B., N.H. and R.M.H. hold founding equity in Cerca Magnetics Limited.

Acknowledgements

Elena Boto, Niall Holmes, Ryan M Hill, Richard Bowtell and Matthew J Brookes are supported by the UK Quantum Technology Hub in Sensing and Timing, funded by the Engineering and Physical Sciences Research Council (EPSRC) (EP/T001046/1), and a Wellcome Collaborative Award in Science (203257/Z/16/Z and 203257/B/16/Z). Xavier De Tiège is Postdoctorate Clinical Master Specialist at the Fonds de la Recherche Scientifique (FRS-FNRS, Brussels, Belgium). Mathieu Bourguignon was supported by the program Attract of Innoviris (grant 2019-BB2B-110).

The SQUID-based and OPM-based MEG projects at the CUB Hôpital Erasme are financially supported by the Fonds Erasme (Brussels, Belgium).

Supplementary materials

Supplementary material associated with this article can be found, in the online version, at doi:10.1016/j.neuroimage.2021.117969.

References

Ahissar, E., Nagarajan, S., Ahissar, M., Protopapas, A., Mahncke, H., Merzenich, M.M., 2001. Speech comprehension is correlated with temporal response patterns recorded from auditory cortex. Proc. Natl. Acad. Sci. 98, 13367–13372.

Ahonen, A.I., Hämäläinen, M.S., Ilmoniemi, R.J., Kajola, M.J., Knuutila, J.E., Simola, J.T., Vilkman, V.A., 1993. Sampling theory for neuromagnetic detector arrays. IEEE Trans. Biomed. Eng. 40, 859–869.

Altarev, I., Babcock, E., Beck, D., Burghoff, M., Chesnevskaya, S., Chupp, T., Degenkolb, S., Fan, I., Fierlinger, P., Frei, A., Gutsmiedl, E., Knappe-Grüneberg, S., Kuchler, F., Lauer, T., Link, P., Lins, T., Marino, M., McAndrew, J., Niessen, B., Paul, S., Petzoldt, G., Schläpfer, U., Schnabel, A., Sharma, S., Singh, J., Stoepler, R., Stuiber, S., Sturm, M., Taubenheim, B., Trahms, L., Voigt, J., Zechlau, T., 2014. A magnetically shielded room with ultra low residual field and gradient. Rev. Sci. Instrum. 85, 075106.

Ashburner, J., Friston, K.J., 1999. Nonlinear spatial normalization using basis functions. Hum. Brain Mapp. 7, 254–266.

Ashburner, J., Neelin, P., Collins, D.L., Evans, A., Friston, K., 1997. Incorporating prior knowledge into image registration. Neuroimage 6, 344–352.

Barry, D.N., Tierney, T.M., Holmes, N., Boto, E., Roberts, G., Leggett, J., Bowtell, R., Brookes, M.J., Barnes, G.R., Maguire, E.A., 2019. Imaging the human hippocampus with optically-pumped magnetoencephalography. Neuroimage 203, 116192.

Biesmans, W., Das, N., Francart, T., Bertrand, A., 2017. Auditory-inspired speech envelope extraction methods for improved EEG-based auditory attention detection in a cocktail party scenario. IEEE Trans. Neural Syst. Rehabil. Eng. 25, 402–412.

Borna, A., Carter, T.R., Goldberg, J.D., Colombo, A.P., Jau, Y.-.Y., Berry, C., McKay, J., Stephen, J., Weisend, M., Schwindt, P.D.D., 2017. A 20-channel magnetoencephalography system based on optically pumped magnetometers. Phys. Med. Biol. 62, 8909–8923.

Bortel, R., Sovka, P., 2014. Approximation of the null distribution of the multiple coherence estimated with segment overlapping. Signal Process. 96, 310–314.

Boto, E., Bowtell, R., Krüger, P., Fromhold, T.M., Morris, P.G., Meyer, S.S., Barnes, G.R., Brookes, M.J., 2016. On the potential of a new generation of magnetometers for MEG: a beamformer simulation study. PLoS ONE 11, e0157655.

Boto, E., Holmes, N., Leggett, J., Roberts, G., Shah, V., Meyer, S.S., Muñoz, L.D., Mullinger, K.J., Tierney, T.M., Bestmann, S., Barnes, G.R., Bowtell, R., Brookes, M.J., 2018. Moving magnetoencephalography towards real-world applications with a wearable system. Nature 555, 657–661.

Boto, E., Meyer, S.S., Shah, V., Alem, O., Knappe, S., Kruger, P., Fromhold, T.M., Lim, M., Glover, P.M., Morris, P.G., Bowtell, R., Barnes, G.R., Brookes, M.J., 2017. A new generation of magnetoencephalography: room temperature measurements using optically-pumped magnetometers. Neuroimage 149, 404–414.

Boto, E., Seedat, Z.A., Holmes, N., Leggett, J., Hill, R.M., Roberts, G., Shah, V., Fromhold, T.M., Mullinger, K.J., Tierney, T.M., Barnes, G.R., Bowtell, R., Brookes, M.J., 2019. Wearable neuroimaging: combining and contrasting magnetoencephalography and electroencephalography. Neuroimage 201, 116099.

Bourguignon, M., Baart, M., Kapnoula, E.C., Molinaro, N., 2020. Lip-reading enables the brain to synthesize auditory features of unknown silent speech. J. Neurosci. 40, 1053–1065.

Bourguignon, M., De Tiège, X., Op de Beeck, M., Ligot, N., Paquier, P., Van Bogaert, P., Goldman, S., Hari, R., Jousmäki, V., 2013. The pace of prosodic phrasing couples the listener's cortex to the reader's voice. Hum. Brain Mapp. 34, 314–326.

Bourguignon, M., Molinaro, N., Wens, V., 2017. Contrasting functional imaging parametric maps: the mislocation problem and alternative solutions. Neuroimage 169, 200–211.

Bourguignon, M., Piitulainen, H., De Tiège, X., Jousmäki, V., Hari, R., 2015. Corticokinematic coherence mainly reflects movement-induced proprioceptive feedback. Neuroimage 106, 382–390.

Bourguignon, M., Whitmarsh, S., Piitulainen, H., Hari, R., Jousmäki, V., Lundqvist, D., 2016. Reliable recording and analysis of MEG-based corticokinematic coherence in the presence of strong magnetic artifacts. Clin. Neurophysiol. 127, 1460–1469.

Broderick, M.P., Anderson, A.J., Di Liberto, G.M., Crosse, M.J., Lalor, E.C., 2017. Electrophysiological correlates of semantic dissimilarity reflect the comprehension of natural, narrative speech. Curr. Biol. 28, 803–809.

Broderick, M.P., Anderson, A.J., Lalor, E.C., 2019. Semantic context enhances the early auditory encoding of natural speech. J. Neurosci. 39, 7564–7575.

Budker, D., Jackson Kimball, D.F., 2013. Optical Magnetometry. Cambridge University Press.

Budker, D., Romalis, M., 2007. Optical magnetometry. Nat. Phys. 3, 227–234.

Carrette, E., De Tiège, X., Op De Beeck, M., De Herdt, V., Meurs, A., Legros, B., Raedt, R., Deblaere, K., Van Roost, D., Bourguignon, M., Goldman, S., Boon, P., Van Bogaert, P., Vonck, K., 2011. Magnetoencephalography in epilepsy patients carrying a vagus nerve stimulator. Epilepsy Res. 93, 44–52.

Chermak, G.D., Musiek, F.E., Craig, C.H., 1997. Central Auditory Processing Disorders: New Perspectives. Singular.

Cherry, E.C., 1953. Some experiments on the recognition of speech, with one and with two ears. J. Acoust. Soc. Am. 25, 975–979.

Colombo, A.P., Carter, T.R., Borna, A., Jau, Y.-.Y., Johnson, C.N., Dagel, A.L., Schwindt, P.D.D., 2016. Four-channel optically pumped atomic magnetometer for magnetoencephalography. Opt. Express 24, 15403–15416.

Coquelet, N., De Tiège, X., Destoky, F., Roshchupkina, L., Bourguignon, M., Goldman, S., Peigneux, P., Wens, V., 2020. Comparing MEG and high-density EEG for intrinsic functional connectivity mapping. Neuroimage 210, 116556.

Crosse, M.J., Di Liberto, G.M., Bednar, A., Lalor, E.C., 2016. The multivariate temporal response function (mTRF) toolbox: a MATLAB toolbox for relating neural signals to continuous stimuli. Front. Hum. Neurosci. 10, 604.

Dale, A.M., Sereno, M.I., 1993. Improved localizadon of cortical activity by combining EEG and MEG with MRI cortical surface reconstruction: a linear approach. J. Cogn. Neurosci. 5, 162–176.

Destoky, F., Bertels, J., Niesen, M., Wens, V., Vander Ghinst, M., Leybaert, J., Lallier, M., Ince, R.A.A., Gross, J., De Tiège, X., Bourguignon, M., 2019a. Cortical tracking of speech in noise accounts for reading strategies in children. PLoS Biol. 18, e3000840.

Destoky, F., Philippe, M., Bertels, J., Verhasselt, M., Coquelet, N., Vander Ghinst, M., Wens, V., De Tiège, X., Bourguignon, M., 2019b. Comparing the potential of MEG and EEG to uncover brain tracking of speech temporal envelope. Neuroimage 184, 201–213.

De Tiège, X., Legros, B., Op de Beeck, M., Goldman, S., Van Bogaert, P., 2008. Vagus nerve stimulation. J. Neurosurg.: Pediatr. 2, 375–377.

Di Liberto, G.M., O'Sullivan, J.A., Lalor, E.C., 2015. Low-frequency cortical entrainment to speech reflects phoneme-level processing. Curr. Biol. 25, 2457–2465.

Di Liberto, G.M., Peter, V., Kalashnikova, M., Goswami, U., Burnham, D., Lalor, E.C., 2018. Atypical cortical entrainment to speech in the right hemisphere underpins phonemic deficits in dyslexia. Neuroimage 175, 70–79.

Ding, N., Patel, A.D., Chen, L., Butler, H., Luo, C., Poeppel, D., 2017. Temporal modulations in speech and music. Neurosci. Biobehav. Rev. 81, 181–187.

Ding, N., Simon, J.Z., 2014. Cortical entrainment to continuous speech: functional roles and interpretations. Front. Hum. Neurosci. 8, 311.

Ding, N., Simon, J.Z., 2012. Emergence of neural encoding of auditory objects while listening to competing speakers. Proc. Natl. Acad. Sci. U. S. A. 109, 11854–11859.

Faes, L., Pinna, G.D., Porta, A., Maestri, R., Nollo, G., 2004. Surrogate data analysis for assessing the significance of the coherence function. IEEE Trans. Biomed. Eng. 51, 1156–1166.

Giraud, A.-.L., Poeppel, D., 2012. Cortical oscillations and speech processing: emerging computational principles and operations. Nat. Neurosci. 15, 511–517.

Goswami, U., 2011. A temporal sampling framework for developmental dyslexia. Trends Cogn. Sci. 15, 3–10.

Goswami, U., Power, A.J., Lallier, M., Facoetti, A., 2014. Oscillatory "temporal sampling" and developmental dyslexia: toward an over-arching theoretical framework. Front. Hum. Neurosci. 8, 904.

Gross, J., Hoogenboom, N., Thut, G., Schyns, P., Panzeri, S., Belin, P., Garrod, S., 2013. Speech rhythms and multiplexed oscillatory sensory coding in the human brain. PLoS Biol 11, e1001752.

Gross, J., Kujala, J., Hamalainen, M., Timmermann, L., Schnitzler, A., Salmelin, R., 2001. Dynamic imaging of coherent sources: studying neural interactions in the human brain. Proc. Natl. Acad. Sci. U. S. A. 98, 694–699.

Halliday, D.M., Rosenberg, J.R., Amjad, A.M., Breeze, P., Conway, B.A., Farmer, S.F., 1995. A framework for the analysis of mixed time series/point process data–theory and application to the study of physiological tremor, single motor unit discharges and electromyograms. Prog. Biophys. Mol. Biol. 64, 237–278.

Hämäläinen, J.A., Rupp, A., Soltész, F., Szücs, D., Goswami, U., 2012. Reduced phase locking to slow amplitude modulation in adults with dyslexia: an MEG study. Neuroimage 59, 2952–2961.

Hämäläinen, M., Hari, R., Ilmoniemi, R.J., Knuutila, J., Lounasmaa, O.V., 1993. Magnetoencephalography—Theory, instrumentation, and applications to noninvasive studies of the working human brain. Rev. Mod. Phys. doi:10.1103/revmodphys.65.413.

Hämäläinen, M.S., Ilmoniemi, R.J., 1994. Interpreting magnetic fields of the brain: minimum norm estimates. Med. Biol. Eng. Comput. 32, 35–42.

Hämäläinen, M.S., Lin, F.-.H., Mosher, J.C., 2010. Anatomically and functionally constrained minimum-norm estimates. In: MEG: An Introduction to Methods, pp. 186–215.

Hari, R., Joutsiniemi, S.-.L., Sarvas, J., 1988. Spatial resolution of neuromagnetic records: theoretical calculations in a spherical model. Electroencephalogr. Clin. Neurophys. /Evoked Potentials Sec. 71, 64–72.

Hill, R.M., Boto, E., Holmes, N., Hartley, C., Seedat, Z.A., Leggett, J., Roberts, G., Shah, V., Tierney, T.M., Woolrich, M.W., Stagg, C.J., Barnes, G.R., Bowtell, R., Slater, R., Brookes, M.J., 2019. A tool for functional brain imaging with lifespan compliance. Nat. Commun. 10, 4785.

Hill, R.M., Boto, E., Rea, M., Holmes, N., Leggett, J., Coles, L.A., Papastavrou, M., Everton, S., Hunt, B.A.E., Sims, D., Osborne, J., Shah, V., Bowtell, R., Brookes, M.J., 2020. Multi-channel whole-head OPM-MEG: helmet design and a comparison with a conventional system. Neuroimage 219, 116995.

Holmes, N., Leggett, J., Boto, E., Roberts, G., Hill, R.M., Tierney, T.M., Shah, V., Barnes, G.R., Brookes, M.J., Bowtell, R., 2018. A bi-planar coil system for nulling background magnetic fields in scalp mounted magnetoencephalography. Neuroimage 181, 760–774.

Holmes, N., Tierney, T.M., Leggett, J., Boto, E., Mellor, S., Roberts, G., Hill, R.M., Shah, V., Barnes, G.R., Brookes, M.J., Bowtell, R., 2019. Balanced, bi-planar magnetic field and field gradient coils for field compensation in wearable magnetoencephalography. Sci. Rep. 9, 14196.

Horton, C., D'Zmura, M., Srinivasan, R., 2013. Suppression of competing speech through entrainment of cortical oscillations. J. Neurophysiol. 109, 3082–3093.

Hyvärinen, A., Karhunen, J., Oja, E., 2001. Independent component analysis.

Iivanainen, J., Mäkinen, A.J., Zetter, R., Stenroos, M., Ilmoniemi, R.J., Parkkonen, L., 2020a. Spatial sampling of MEG and EEG revisited: from spatial-frequency spectra to model-informed sampling. arXiv 2006. 02919.

Iivanainen, J., Stenroos, M., Parkkonen, L., 2017. Measuring MEG closer to the brain: performance of on-scalp sensor arrays. Neuroimage 147, 542–553.

Iivanainen, J., Zetter, R., Grön, M., Hakkarainen, K., Parkkonen, L., 2019. On-scalp MEG system utilizing an actively shielded array of optically-pumped magnetometers. Neuroimage 194, 244–258.

Iivanainen, J., Zetter, R., Parkkonen, L., 2020b. Potential of on-scalp MEG: robust detection of human visual gamma-band responses. Hum. Brain Mapp. 41, 150–161.

Kakisaka, Y., Mosher, J.C., Wang, Z.I., Jin, K., Dubarry, A.-.S., Alexopoulos, A.V., Burgess, R.C., 2013. Utility of temporally-extended signal space separation algorithm for magnetic noise from vagal nerve stimulators. Clin. Neurophysiol. 124, 1277–1282.

Keitel, A., Gross, J., Kayser, C., 2018. Perceptually relevant speech tracking in auditory and motor cortex reflects distinct linguistic features. PLoS Biol 16, e2004473.

Kösem, A., van Wassenhove, V., 2016. Distinct contributions of low- and high-frequency neural oscillations to speech comprehension. Lang., Cogn. Neurosci. 32, 536–544.

Lalor, E.C., Foxe, J.J., 2010. Neural responses to uninterrupted natural speech can be extracted with precise temporal resolution. Eur. J. Neurosci. 31, 189–193.

Lin, C.-.H., Tierney, T.M., Holmes, N., Boto, E., Leggett, J., Bestmann, S., Bowtell, R., Brookes, M.J., Barnes, G.R., Chris Miall, R., 2019. Using optically-pumped magnetometers to measure magnetoencephalographic signals in the human cerebellum. J. Physiol. 597, 4309–4324.

Lizarazu, M., Lallier, M., Molinaro, N., Bourguignon, M., Paz-Alonso, P.M., Lerma-Usabiaga, G., Carreiras, M., 2015. Developmental evaluation of atypical auditory sampling in dyslexia: functional and structural evidence. Hum. Brain Mapp. 36, 4986–5002.

Luo, H., Poeppel, D., 2007. Phase patterns of neuronal responses reliably discriminate speech in human auditory cortex. Neuron 54, 1001–1010.
Mäkelä, J.P., Taulu, S., Pohjola, J., Ahonen, A., Pekkonen, E., 2007. Effects of subthalamic nucleus stimulation on spontaneous sensorimotor MEG activity in a Parkinsonian patient. Int. Congress Ser. 1300, 345–348.
Mesgarani, N., David, S.V., Fritz, J.B., Shamma, S.A., 2009. Influence of context and behavior on stimulus reconstruction from neural activity in primary auditory cortex. J. Neurophysiol. 102, 3329–3339.
Meyer, L., 2018. The neural oscillations of speech processing and language comprehension: state of the art and emerging mechanisms. Eur. J. Neurosci. 48, 2609–2621.
Meyer, L., Gumbert, M., 2018. Synchronization of electrophysiological responses with speech benefits syntactic information processing. J. Cogn. Neurosci. 1–10.
Molinaro, N., Lizarazu, M., Lallier, M., Bourguignon, M., Carreiras, M., 2016. Out-of-synchrony speech entrainment in developmental dyslexia. Hum. Brain Mapp. 37, 2767–2783.
Müller, J.A., Kollmeier, B., Debener, S., Brand, T., 2018. Influence of auditory attention on sentence recognition captured by the neural phase. Eur. J. Neurosci. 51, 1305–1314.
Muthukumaraswamy, S.D., 2013. High-frequency brain activity and muscle artifacts in MEG/EEG: a review and recommendations. Front. Hum. Neurosci. 7, 138.
Nardelli, N.V., Krzyzewski, S.P., Knappe, S.A., 2019. Reducing crosstalk in optically-pumped magnetometer arrays. Phys. Med. Biol. 64, 21NT03.
Nichols, T.E., Holmes, A.P., 2002. Nonparametric permutation tests for functional neuroimaging: a primer with examples. Hum. Brain Mapp. 15, 1–25.
Nolte, G., 2003. The magnetic lead field theorem in the quasi-static approximation and its use for magnetoencephalography forward calculation in realistic volume conductors. Phys. Med. Biol. 48, 3637–3652.
Oldfield, R.C., 1971. The assessment and analysis of handedness: the Edinburgh inventory. Neuropsychologia 9, 97–113.
Oostenveld, R., Fries, P., Maris, E., Schoffelen, J.-.M., 2011. FieldTrip: open source software for advanced analysis of MEG, EEG, and invasive electrophysiological data. Comput. Intell. Neurosci. 2011, 156869.
Osborne, J., Orton, J., Alem, O., Shah, V., 2018. Fully integrated, standalone zero field optically pumped magnetometer for biomagnetism. Steep Dispers. Eng. Opto-Atomic Precis. Metrol. XI 10548, 1G.
O'Sullivan, J.A., Power, A.J., Mesgarani, N., Rajaram, S., Foxe, J.J., Shinn-Cunningham, B.G., Slaney, M., Shamma, S.A., Lalor, E.C., 2014. Attentional selection in a cocktail party environment can be decoded from single-trial EEG. Cereb. Cortex 25, 1697–1706.
Park, H., Ince, R.A.A., Schyns, P.G., Thut, G., Gross, J., 2015. Frontal top-down signals increase coupling of auditory low-frequency oscillations to continuous speech in human listeners. Curr. Biol. doi:10.1016/j.cub.2015.04.049.
Peelle, J.E., Gross, J., Davis, M.H., 2013. Phase-locked responses to speech in human auditory cortex are enhanced during comprehension. Cereb. Cortex 23, 1378–1387.
Pellegrino, F., Coupé, C., Marsico, E., 2011. Across-language perspective on speech information rate. Language (Baltim) 87, 539–558.
Power, A.J., Foxe, J.J., Forde, E.-.J., Reilly, R.B., Lalor, E.C., 2012. At what time is the cocktail party? A late locus of selective attention to natural speech. Eur. J. Neurosci. 35, 1497–1503.
Puschmann, S., Steinkamp, S., Gillich, I., Mirkovic, B., Debener, S., Thiel, C.M., 2017. The right temporoparietal junction supports speech tracking during selective listening: evidence from concurrent EEG-fMRI. J. Neurosci. 37, 11505–11516.
Rosen, S., 1992. Temporal information in speech: acoustic, auditory and linguistic aspects. Philos. Trans. R. Soc. Lond. B Biol. Sci. 336, 367–373.
Sekihara, K., Sahani, M., Nagarajan, S.S., 2005. Localization bias and spatial resolution of adaptive and non-adaptive spatial filters for MEG source reconstruction. Neuroimage 25, 1056–1067.
Shah, V.K., Wakai, R.T., 2013. A compact, high performance atomic magnetometer for biomedical applications. Phys. Med. Biol. 58, 8153–8161.
Song, T., Cui, L., Gaa, K., Feffer, L., Taulu, S., Lee, R.R., Huang, M., 2009. Signal space separation algorithm and its application on suppressing artifacts caused by vagus nerve stimulation for magnetoencephalography recordings. J. Clin. Neurophysiol. 26, 392–400.
Stolk, A., Todorovic, A., Schoffelen, J.-.M., Oostenveld, R., 2013. Online and offline tools for head movement compensation in MEG. Neuroimage 68, 39–48.
Tanaka, N., Thiele, E.A., Madsen, J.R., Bourgeois, B.F., Stufflebeam, S.M., 2009. Magnetoencephalographic Analysis in Patients With Vagus Nerve Stimulator. Pediatr. Neurol. 41, 383–387.
Taulu, S., Hari, R., 2009. Removal of magnetoencephalographic artifacts with temporal signal-space separation: demonstration with single-trial auditory-evoked responses. Hum. Brain Mapp. 30, 1524–1534.
Taulu, S., Kajola, M., Simola, J., 2004. Suppression of interference and artifacts by the signal space separation method. Brain Topogr. 16, 269–275.
Taulu, S., Simola, J., 2006. Spatiotemporal signal space separation method for rejecting nearby interference in MEG measurements. Phys. Med. Biol. 51, 1759–1768.
Taulu, S., Simola, J., Kajola, M., 2005. Applications of the signal space separation method. IEEE Trans. Signal Process. 53, 3359–3372.
Thiede, A., Glerean, E., Kujala, T., Parkkonen, L., 2020. Atypical MEG inter-subject correlation during listening to continuous natural speech in dyslexia. Neuroimage 216, 116799.
Tierney, T.M., Holmes, N., Mellor, S., López, J.D., Roberts, G., Hill, R.M., Boto, E., Leggett, J., Shah, V., Brookes, M.J., Bowtell, R., Barnes, G.R., 2019a. Optically pumped magnetometers: from quantum origins to multi-channel magnetoencephalography. Neuroimage 199, 598–608.
Tierney, T.M., Holmes, N., Meyer, S.S., Boto, E., Roberts, G., Leggett, J., Buck, S., Duque-Muñoz, L., Litvak, V., Bestmann, S., Baldeweg, T., Bowtell, R., Brookes, M.J., Barnes, G.R., 2018. Cognitive neuroscience using wearable magnetometer arrays: non-invasive assessment of language function. Neuroimage 181, 513–520.
Tierney, T.M., Mellor, S., O'Neill, G.C., Holmes, N., Boto, E., Roberts, G., Hill, R.M., Leggett, J., Bowtell, R., Brookes, M.J., Barnes, G.R., 2019b. Pragmatic spatial sampling for wearable MEG arrays. BioRxiv 890426.
Vander Ghinst, M., Bourguignon, M., Niesen, M., Wens, V., Hassid, S., Choufani, G., Jousmäki, V., Hari, R., Goldman, S., De Tiège, X., 2019. Cortical tracking of speech-in-noise develops from childhood to adulthood. J. Neurosci. 39, 2938–2950.
Vander Ghinst, M., Bourguignon, M., Op de Beeck, M., Wens, V., Marty, B., Hassid, S., Choufani, G., Jousmäki, V., Hari, R., Van Bogaert, P., Goldman, S., De Tiège, X., 2016. Left superior temporal gyrus is coupled to attended speech in a cocktail-party auditory scene. J. Neurosci. 36, 1596–1606.
Varoquaux, G., Raamana, P.R., Engemann, D.A., Hoyos-Idrobo, A., Schwartz, Y., Thirion, B., 2017. Assessing and tuning brain decoders: cross-validation, caveats, and guidelines. Neuroimage 145, 166–179.
Vigario, R., Sarela, J., Jousmiki, V., Hamalainen, M., Oja, E., 2000. Independent component approach to the analysis of EEG and MEG recordings. IEEE Trans. Biomed. Eng. 47, 589–593.
Wens, V., Marty, B., Mary, A., Bourguignon, M., Op de Beeck, M., Goldman, S., Van Bogaert, P., Peigneux, P., De Tiège, X., 2015. A geometric correction scheme for spatial leakage effects in MEG/EEG seed-based functional connectivity mapping. Hum. Brain Mapp. 36, 4604–4621.
Wyllie, R., Kauer, M., Smetana, G.S., Wakai, R.T., Walker, T.G., 2012. Magnetocardiography with a modular spin-exchange relaxation-free atomic magnetometer array. Phys. Med. Biol. 57, 2619–2632.
Xia, H., Ben-Amar Baranga, A., Hoffman, D., Romalis, M.V., 2006. Magnetoencephalography with an atomic magnetometer. Appl. Phys. Lett. 89, 211104.
Zion-Golumbic, E.M., Ding, N., Bickel, S., Lakatos, P., Schevon, C.A., McKhann, G.M., Goodman, R.R., Emerson, R., Mehta, A.D., Simon, J.Z., Poeppel, D., Schroeder, C.E., 2013. Mechanisms underlying selective neuronal tracking of attended speech at a "cocktail party. Neuron 77, 980–991.